UCLA
UCLA Previously Published Works

Title

The effect of scaffold macroporosity on angiogenesis and cell survival in tissue-engineered smooth muscle

Permalink

https://escholarship.org/uc/item/2t0305tr

Journal

Biomaterials, 35(19)

ISSN

0267-6605

Authors

Walthers, Christopher M
Nazemi, Alireza K
Patel, Shilpy L
et al.

Publication Date

2014-06-01

DOI

10.1016/j.biomaterials.2014.03.025

Peer reviewed

eScholarship.org Powered by the California Digital Library
University of California

NIH Public Access
Author Manuscript
Biomaterials. Author manuscript; available in PMC 2015 June 01.

Published in final edited form as:
Biomaterials. 2014 June ; 35(19): 5129–5137. doi:10.1016/j.biomaterials.2014.03.025.

The Effect of Scaffold Macroporosity on Angiogenesis and Cell Survival in Tissue-Engineered Smooth Muscle

Christopher M. Walthers, M.S.[1], **Alireza Nazemi, B.S.**[1], **Shilpy Patel, B.S.**[1], **Benjamin Wu, D.D.S., Ph.D.**[1,2], and **James C.Y. Dunn, M.D., Ph.D.**[*,1,3]

[1]Department of Bioengineering, University of California, Los Angeles, CA

[2]Department of Advanced Prosthodontics, Biomaterials, and Hospital Dentistry, University of California, Los Angeles, CA

[3]Department of Surgery, University of California, Los Angeles, CA

Abstract

Angiogenesis and survival of cells within thick scaffolds is a major concern in tissue engineering. The purpose of this study is to increase the survival of intestinal smooth muscle cells (SMCs) in implanted tissue-engineered constructs. We incorporated 250-μm pores in multi-layered, electrospun scaffolds with a macroporosity ranging from 15% to 25% to facilitate angiogenesis. The survival of green fluorescent protein (GFP)-expressing SMCs was evaluated after 2 weeks of implantation. Whereas host cellular infiltration was similar in scaffolds with different macroporosities, blood vessel development increased with increasing macroporosity. Scaffolds with 25% macropores had the most GFP-expressing SMCs, which correlated with the highest degree of angiogenesis over 1 mm away from the outermost layer. The 25% macroporous group exceeded a critical threshold of macropore connectivity, accelerating angiogenesis and improving implanted cell survival in a tissue-engineered smooth muscle construct.

Introduction

Many tissue engineering applications employ scaffolds seeded with cells that grow during *in vitro* culture prior to implantation. In recent years, there have been many advances in tissue engineering of three-dimensional scaffolds. In such large scaffolds, the diffusion of nutrients and oxygen becomes an important consideration, and rapid vascular infiltration is necessary

© 2014 Elsevier Ltd. All rights reserved.

[*]Address correspondence to: Department of Bioengineering University of California, Los Angeles 420 Westwood Plaza Room 5121 Engineering V Los Angeles, CA 90095 jdunn@mednet.ucla.edu.

Publisher's Disclaimer: This is a PDF file of an unedited manuscript that has been accepted for publication. As a service to our customers we are providing this early version of the manuscript. The manuscript will undergo copyediting, typesetting, and review of the resulting proof before it is published in its final citable form. Please note that during the production process errors may be discovered which could affect the content, and all legal disclaimers that apply to the journal pertain.

Author and Co-author Contact Information: Walthers, CM Department of Bioengineering University of California, Los Angeles Los Angeles, CA 90095 United States of America
Nazemi, A Department of Bioengineering University of California, Los Angeles Los Angeles, CA 90095 United States of America
Patel, S Department of Bioengineering University of California, Los Angeles Los Angeles, CA 90095 United States of America
Wu, BM Department of Bioengineering University of California, Los Angeles Los Angeles, CA 90095 United States of America

NIH-PA Author Manuscript
NIH-PA Author Manuscript
NIH-PA Author Manuscript

NIH-PA Author Manuscript

NIH-PA Author Manuscript

NIH-PA Author Manuscript

in vivo to sustain seeded cells following implantation [1]. By diffusion alone, thick scaffolds can only sustain cells within a few hundred μm of the liquid-scaffold interface *in vitro*, a limitation which is closely approximated *in vivo* [2,3]. Various techniques to improving vascular conduction have been studied [4], including use of growth factors [5–7], bioactive materials [8,9], microfabrication [10–12], angiogenic cells [13–15], decellularized organs with intact microvasculature [16,17], non-biological factors [18], and even oxygen-producing biomaterials [19]. Microfabrication is especially important since improved conduction pathways can accelerate or improve other efforts to increase angiogenesis in implants [20].

Porosity of scaffolds used in tissue engineering have long been known to affect angiogenesis and the development of functional tissue including structural tissues such as bone [21,22] and cartilage [23,24], as well as soft tissues such as the urethra [25], liver [26], skin [27,28], muscle [29], vascular structures [30], and soft tissue fillers [31]. In a previous report, we explored the role of pore size in electrospun polycaprolactone scaffolds using lasercut holes of various diameter ranging from 80 to 300 μm while maintaining a 15% macroporosity by area [32]. Larger diameter pores led to an increase in cellular infiltration and vascular development compared to controls without a significant change in material properties.In that study, the optimal density of the 300-μm pores, however, was not explored. Ideally, a porous electrospun scaffolds should have a large surface area for cell attachment, yet enough macropores to allow rapid angiogenesis. The density of macropores necessary to allow sufficient angiogenesis to sustain implanted cell survival within electrospun scaffolds remains unclear [33].

Many diseases affecting the gastrointestinal tract leave insufficient functioning intestine for normal absorption, resulting in a condition known as intestinal failure [34]. Without methods for curing these conditions, medical options are limited to reducing symptoms, contributing to unacceptably high morbidity and mortality rates [35,36]. Tissue engineering is an appealing alternative for creating new intestine. While much progress has been made on growing the intestinal epithelium, less has been done with the intestinal smooth muscle [37–39]. The intestinal smooth muscle is a multi-layered tissue composed of an inner circular layer beneath the submucosa and an outer longitudinal layer adjacent to the serosa. Smooth muscle is critical for the transport of waste and nutrients through the gastrointestinal tract. Functional tissue-engineered smooth muscle that can generate the contraction strength necessary for peristalsis has been difficult to produce. Even the strongest tissue-engineered muscles are much weaker than normal muscle, suggesting the need for thicker scaffolds, which will further increase the need for rapid vascular infiltration and better mimic of the multi-layered intestine [1,33,40,41]. Furthermore, survival and maturity of intestinal smooth muscle cells (SMCs) *in vivo* is accompanied by angiogenesis [42,43], suggesting that a pro-angiogenic biomaterial may enable the development of a mature smooth muscle.

We sought to determine the optimal macroporosity to generate a critical amount of angiogenesis necessary to sustain a population of implanted SMCs within multi-layered scaffolds. Macroporosity was generated by laser-cutting of electrospun sheets, and cell-seeded sheets were rolled into a multi-layered tube. Following 2 weeks of implantation, the

NIH-PA Author Manuscript

NIH-PA Author Manuscript

NIH-PA Author Manuscript

scaffolds were evaluated for cellular infiltration, vascular in-growth, and survival of implanted GFP-expressing SMCs.

Materials and Methods

2.1 Fabrication of poly ε-caprolactone (PCL) scaffolds

Polymer solution was made from 11% w/w ester capped PCL (Lactel Absorbable Polymers, Birmingham, AL) in hexafluoro-2-propanol (Sigma, St. Louis, MO). Our electrospinning technique was described in detail previously [32]. Following the electrospinning, the designs of PCL scaffolds were drawn with Adobe Illustrator, and scaffolds were cut from the whole electrospun PCL sheet using a VersaLASER 2.3 laser cutting system (Universal Laser Systems, Scottsdale, AZ). Scaffolds for *in vivo* experiments were fabricated with a regular pattern to create pores in the PCL sheet. The pattern was drawn with 150-μm circles to accommodate melting, which created 250-μm pores with a 75-μm thick ring of solid polymer melt around the perimeter. After the pores were made, a second pattern was run to cut the perimeter of the scaffold to create a rectangular 45 mm × 9.5 mm sheet. Rows of pores were offset to create a staggered series of columns, and the distance between each pore was varied to create different porosities. Additionally, each row was 0.5 mm below the previous row. The laser was set to a power of 25x and a speed of 50x, with three consecutive scans over each substrate.

2.2 Macroporosity Measurements

Scaffold macroporosity was determined using a VHX-2000 digital microscope (Keyence, Itasca, IL). Three images of each scaffold were taken at 300x magnification. Macroporosity was determined using ImageJ software to threshold and calculate the area lacking polymer in each picture.

2.3 Collagen Coating

PCL scaffolds were loaded into a plasma chamber (Harrick Plasma, Ithaca, NY), at 500 mTorr and were etched for 1.5 minutes at high power. Scaffolds were then sterilized in 70% ethanol for 30 minutes, rehydrated with decreasing percentages of ethanol and finally in phosphate buffered saline (PBS). Scaffolds were then immediately coated overnight at 37°C with 500 μL of a 0.25 mg/mL collagen (Purecol, Advanced Biomatrix, San Diego, CA) solution neutralized with .1N sodium hydroxide to pH 7.4 and diluted in PBS. The coated scaffolds were rinsed 3 times in PBS for 5 minutes and then soaked in cell-culture medium until cell seeding.

2.4 GFP-expressing SMC Seeding of the Scaffold

2.4.1 Culture of GFP-expressing SMCs—Transgenic GFP-expressing Lewis rats were obtained from a breeding colony maintained by UCLA's Department of Laboratory Animal Medicine and were sacrificed with approval of Institutional Review Board. SMC isolation was described in a previous publication [44]. Following digestion, collagenase was quenched in cell-culture medium consisting of Dulbecco's Modified Eagle's Media (DMEM, Life Technologies, Carlsbad, CA) with 10% Fetal Bovine Serum (FBS, Life Technologies), and 1x ABAM (Life Technologies).

NIH-PA Author Manuscript

NIH-PA Author Manuscript

NIH-PA Author Manuscript

2.4.2 GFP-expressing SMC Seeding—Primary SMCs were counted with a hemacytometer and were seeded at 250,000 cells/cm^2 on PCL scaffolds within a custom polydimethylsiloxane (PDMS, Dow Corning, Elizabethtown, KY) cell seeding tray shaped to fit the scaffolds. Cell-culture medium was changed every two days after washing with PBS and scaffolds were maintained in a 37°C humidified incubator with 10% carbon dioxide for two weeks prior to implantation.

2.5 Scaffold Implantation

2.5.1 Scaffold preparation—On the day of implantation, scaffolds containing cells were washed once with PBS, and a 9.5 mm section of sterile #6 silicone catheter (Bard, Covington, GA) was used to provide structural support for wrapping the scaffold in to a multi-layered tube. The catheter formed the lumen of the tube and prevented the scaffold from collapsing. Each scaffold was wrapped six times around the catheter with the cell-seeded side facing outwards. After wrapping, each scaffold was secured to the catheter with a 6-0 prolene suture (Ethicon, San Angelo, TX) and the ends were plugged with silicone rubber (Dow Corning, Midland, MI) to prevent cell infiltration from the scaffold edges. The rolled scaffolds were rinsed and stored in DMEM on ice until implantation. Scaffold wrapping is demonstrated in Figure 2.

2.5.2 Implantation—All surgical procedures were done in accordance with UCLA's Animal Research Committee protocol # 2004-197-21. The surgical procedure was described in detail in a previous publication [32]. At specimen retrieval, each scaffold was cut in to four equal-sized cylinders, and two segments were used for qPCR while the other two were fixed in formalin for histology.

2.6 Immunohistochemistry

2.6.1 Immunostaining of GFP-expressing SMCs—The scaffolds fixed in formalin were processed for paraffin embedding and sectioning by UCLA's Translational Pathology Core Laboratory (TPCL). Slides were stained with hematoxylin and eosin (H&E). Normal intestine and GFP-expressing adult intestine were fixed, sectioned, and stained as controls. Each sample was cut into 5-μm sections with two sections per slide; one section on each slide was used for staining, while the second was used as a control with no primary antibody added. Slides were washed with xylene to strip away the paraffin and rehydrated with progressively decreasing concentrations of ethanol in water.

For immunofluorescence, antigen retrieval was performed in Citra solution (Biogenix, Fremont, CA) for 20 minutes at 100°C followed by 20 minutes of cooling at room temperature. Samples were permeabilized with 0.5% Triton X and were washed with PBS-tween twice. A hydrophobic barrier was traced around all samples with a PAP pen (Abcam, Cambridge, MA). Non-specific staining was blocked with a solution of 2% bovine serum albumin and 4% goat serum in PBS-tween for one hour. Following blocking, slides were incubated overnight at 4°C in primary antibody diluted 1:50 in blocking solution. Antibodies for GFP were purchased from Clontech (Mountain View, CA). Excess primary antibody was washed away with three more PBS-tween rinses before a 30 minute incubation with Alexafluor 488 goat anti-mouse secondary (Life Technologies) diluted 1:200 in blocking

NIH-PA Author Manuscript

NIH-PA Author Manuscript

NIH-PA Author Manuscript

solution. Finally, slides were rinsed three more times in PBS-tween before adding a mounting media with added DAPI (Vector, Burlingame, CA) to facilitate nuclei visualization. Fluorescent images were taken with an Olympus IX71 microscope with cellSens software (Olympus, Center Valley, PA).

2.6.2 Immunohistochemical Staining of Von-Williebrand Factor—

Immunohistological staining for von-Willebrand Factor (vWF) was performed to quantify blood vessel infiltration in the scaffolds. Following paraffin removal in xylene and rehydration in decreasing concentrations of ethanol, antigen retrieval was performed in 0.05% trypsin-EDTA solution (Life Technologies) in PBS at 37°C for 15 minutes. Slides were rinsed in PBS and the endogenous peroxidase activity was blocked with 1% hydrogen peroxide in methanol for 30 minutes before drawing a hydrophobic barrier around each section. Samples were again rinsed in PBS and incubated for 1 hour in blocking solution consisting of 4% horse serum and 2% BSA in PBS-tween. Immediately after blocking, samples were incubated overnight in a 1:500 dilution of polyclonal rabbit anti-human vWF antibody (Dako, Carpinteria, CA) in blocking solution. Biotinylated horse anti-rabbit secondary antibodies (Vector Labs, Burlingame, CA) were diluted 1:200 in blocking solution and incubated for 30 minutes at room temperature prior to a 30-minute incubation in horseradish peroxidase streptavidin (Vector). Finally, 3,3′-Diaminobenzidine (DAB) chromogen (Vector) was developed for 10 minutes before counterstaining in hematoxylin. Lastly, samples coverslipped with VectaMount (Vector).

2.6.3 Quantification of Staining—Fluorescent images of DAPI- or GFP- stained sections were taken from four sides of each scaffold section for each implant. Scaffold images were then manually separated in to three parts representing the outermost (“serosal”) two layers, the middle two layers (“middle”), and the innermost (“luminal”) layers. Each part was quantified by area using ImageJ. The four images from each section were added, and the area for each section was averaged with all the sections for the same macroporosity implants. Following staining for vWF, bright field images were taken and separated in the same manner as the fluorescent images. Blood vessels showing positive staining for vWF were counted manually and added to the other images from each section. All sections for each macroporosity implant were used to calculate the mean and standard deviation.

2.7 DNA Extraction and Quantitative Polymerase Chain Reaction

GFP-expressing DNA was collected and quantified using techniques published in previous literature [45]. DNA was extracted from a quarter section of scaffold adjacent to the midline using a DNeasy kit for blood/tissue (Qiagen, Germantown, MD). GFP cell quantity in each scaffold was quantified using DNA extracted from known standards of GFP-expressing SMCs from the same cell harvest. The number of GFP-expressing SMC from each section of scaffold was used to determine that for the entire implant by multiplying by four.

NIH-PA Author Manuscript

NIH-PA Author Manuscript

NIH-PA Author Manuscript

Results

Scaffold Macroporosity Characterization

A fine network of electrospun PCL fibers 2-3 μm in diameter was observed in all scaffolds (Fig. 1). A 75-μm ring of melted polymer circumscribed the 250-μm pores (Fig. 2). Laser-cut scaffolds had an average macroporosity of 15.9% ± 1.4 (designated as “15%”), 19.3% ± 1.4 (“20%”), and 25.1 ± 2.0 (“25%”), while uncut scaffolds had a measured macroporosity of 0.2% ± 0.3 (“0%”).

Histology of retrieved implants

After two weeks of implantation, histologic sections of retrieved implants revealed similar cellular penetration among all scaffolds with macropores (Fig. 3). In contrast, non-porous scaffolds had little cellular penetration through the outermost layer, and the inner layers shriveled due to a lack of cellular support. At higher magnification, cells were observed to fill macropores and aligned along with the fibers of the scaffolds between layers. Most layers within the 20% and 25% macroporous scaffolds and the outer layers of the 15% macroporous scaffolds exhibited swelling similar to that seen previously [32]. The macropores were flanked by the melted ring as a curved edge surrounding the cellular infiltrate (Fig. 3).

Nuclear staining to quantify cellular penetration

Following implantation for two weeks, cell nuclei staining with DAPI revealed more cellular penetration in all layers of each macroporous scaffold when compared to the uncut scaffolds (Fig. 4). There was no statistical difference in cellular penetration between any of the macroporous scaffolds through any of the layers (Fig. 5).

Quantification of angiogenesis

Differences in angiogenesis were visualized with staining for vWF. Blood vessels showed a ring of dark brown vWF-positive staining (Fig. 6). There was a continued increase in vWF staining as the macroporosity increased in the laser-cut scaffolds (Fig. 7).

Quantification of GFP-expressing SMC

Following two weeks implantation, GFP-expressing SMCs were quantified by real-time PCR of GFP DNA in the scaffold. Both the 20% and 25% macroporous scaffolds had a significantly higher number of GFP cells as compared to the uncut scaffolds (Fig. 8). The distribution of GFP-expressing cells within the scaffolds was examined by immunofluorescent staining (Fig. 9). A statistically significant increase in GFP-expressing cells was observed in every layer of the 25% macroporous scaffolds as compared to either the 20% or the 15% macroporous scaffolds (Fig. 10).

Discussion

This study underscores the importance scaffold design conducive to angiogenesis. By increasing scaffold macroporosity by 5%, a roughly three-fold increase in implanted cell survival was achieved. SMCs were able to survive at a distance of over 1 mm from the outer

NIH-PA Author Manuscript

NIH-PA Author Manuscript

NIH-PA Author Manuscript

edge of the 25% macroporous implants, suggesting that even larger implants may be sustainable. Future research will be conducted to determine the functionality and contractile strength of these tissue-engineered smooth muscles. Whether 25% macroporosity represents the optimal porosity for implanted cell survival remains to be determined. While higher macroporosities may lead to an even larger increase in the survival of GFP-expressing SMCs, the scaffolds' surface area available for SMC attachment will limit the density of the macropores. By fine tuning scaffold's macroporosity, we were able to improve angiogenesis significantly in tissue-engineered smooth muscle.

Techniques to microfabricate scaffolds to enhance vascularization are crucial in tissue engineering. Diffusion-limitation is a consistent problem in tissue engineering, and scaffolds of any reasonable magnitude that fail to account for diffusion will ultimately suffer from areas of hypoxia [1,2]. Furthermore, microfabrication is inexpensive, reproducible, fast, and complementary to other efforts to sustain implanted cells [20]. To address the difficulties of creating a thick, multi-layered smooth muscle, we created a sheet of electrospun PCL that was seeded with cells, grown in an incubator, and rolled in to a tube thicker than 1 mm. In these implants, a qualitative cell alignment along scaffold fibers can be observed in higher magnifications (Fig. 3). Two layers of aligned electrospun sheets offset at right angles would provide a similar alignment pattern to the circular and longitudinal smooth muscle found in native intestine. These layers could also create the necessary intra-muscularis niche for intestinal pacemaker and neural cells, potentially leading to peristalsis within the tissue-engineered intestine [46]. For these reasons, electrospun scaffolds with pro-angiogenic macropores are an interesting biomaterial for engineering artificial intestine.

Surface characteristics of fibrous scaffolds such as those formed with electrospinning influence characteristics of cells cultured on the surface, including differentiation [47,48] and behavior [49–53]. It is also well known that electrospun sheets can be a tremendous barrier to cellular and vascular penetration [32,54]. In this study, we showed that vascularity but not total cellularity correlated with the implanted cell survival. The most porous scaffolds in this study were associated with the greatest blood vessel growth and highest number of surviving GFP-expressing SMCs. Implanted GFP-expressing cells were distributed throughout the 25% macroporous scaffolds, suggesting that blood vessel infiltration was either rapid enough to sustain cells up to 1 mm away from the outer omentum, or GFP-expressing cells were able to proliferate and migrate along with infiltrating blood vessels within the 2-week period.

A possible explanation for the difference in implanted cell survival observed in various macroporous scaffolds is that blood vessel infiltration happens more rapidly as the density of the macropores increases. Even though host cells exist in high amounts after two weeks in all scaffolds, the implanted cells may have died in the scaffolds with fewer macropores. Our results suggest that a small increase beyond a threshold macroporosity results in a large increase in implanted cell survival. Additional insight is provided by an analogy to the mathematical percolation theory, the study of network connectivity and the transmittance of substances or information due to network architecture [55]. Percolation theory predicts that past a critical threshold, a series of connections can lead to a percolating cluster, or a phenomenon where sufficient connections exist to conduct passage through a material where

NIH-PA Author Manuscript

NIH-PA Author Manuscript

NIH-PA Author Manuscript

such passage was impossible with slightly fewer connections [56]. Similar analogies to percolation theory exist in biological systems relating to antigen-antibody reactions, lymphocyte membrane network formations, immunology, and conductivity in biological materials [56]. Developing a percolation theory approach to improving blood vessel networks in engineered tissues is an area for future research.

Conclusion

In this study, we demonstrate that a critical threshold macroporosity exists within tissue-engineered smooth muscle constructs. Our findings show that higher macroporosities were significantly more conducive to *in vivo* blood vessel infiltration. We provide evidence that a small increase beyond a threshold macroporosity results in a large increase in SMC survival and angiogenesis. Tissue-engineered smooth muscle constructs thicker than 1 mm were sustained in scaffolds above a critical macroporosity threshold. Our study underscores the importance of pore connectivity within microfabricated scaffolds for tissue engineering.

Acknowledgments

The authors thank Doug Arneson, Elvin Chiang, Abigail Corrin, Arjun Mehta, and Brian Warren for their generous help. This work was supported by an R01 DK083119 from the National Institutes of Health.

References

1. Karande TS, Ong JL, Agrawal CM. Diffusion in musculoskeletal tissue engineering scaffolds: design issues related to porosity, permeability, architecture, and nutrient mixing. Ann Biomed Eng. 2004; 32(12):1728–43. [PubMed: 15675684]
2. Ishaug SL, Crane GM, Miller MJ, Yasko AW, Yaszemski MJ, Mikos AG. Bone formation by three-dimensional stromal osteoblast culture in biodegradable polymer scaffolds. J Biomed Mater Res. 1997; 36(1):17–28. [PubMed: 9212385]
3. Dunn JCY, Chan W-Y, Cristini V, Kim JS, Lowengrub J, Singh S, et al. Analysis of cell growth in three-dimensional scaffolds. Tissue Eng. 2006; 12(4):705–16. [PubMed: 16674285]
4. Kaully T, Kaufman-Francis K, Lesman A, Levenberg S. Vascularization--the conduit to viable engineered tissues. Tissue Eng Part B Rev. 2009; 15(2):159–69. [PubMed: 19309238]
5. Singh S, Wu BM, Dunn JCY. Delivery of VEGF using collagen-coated polycaprolactone scaffolds stimulates angiogenesis. J Biomed Mater Res A. 2012; 100(3):720–7. [PubMed: 22213643]
6. Demirdögen B, Elçin AE, Elçin YM. Neovascularization by bFGF releasing hyaluronic acid-gelatin microspheres: in vitro and in vivo studies. Growth Factors. 2010; 28(6):426–36. [PubMed: 20854186]
7. Matsui M, Tabata Y. Enhanced angiogenesis by multiple release of platelet-rich plasma contents and basic fibroblast growth factor from gelatin hydrogels. Acta Biomater. 2012; 8(5):1792–801. [PubMed: 22293581]
8. Singh S, Wu BM, Dunn JCY. The enhancement of VEGF-mediated angiogenesis by polycaprolactone scaffolds with surface cross-linked heparin. Biomaterials. 2011; 32(8):2059–69. [PubMed: 21147501]
9. Zachman AL, Crowder SW, Ortiz O, Bronikowski CM, Yu SS, Giorgio TD, et al. Pro-angiogenic and anti-inflammatory regulation by functional peptides loaded in polymeric implants for soft tissue regeneration. Tissue Eng Part A. 2013; 19(3 and 4):437–47. [PubMed: 22953721]
10. Wray LS, Tsioris K, Gi ES, Omenetto FG, Kaplan DL. Slowly degradable porous silk microfabricated scaffolds for vascularized tissue formation. Adv Funct Mater. 2013; 23(27):3404–12. [PubMed: 24058328]

NIH-PA Author Manuscript

NIH-PA Author Manuscript

NIH-PA Author Manuscript

11. Chiu LLY, Montgomery M, Liang Y, Liu H, Radisic M. Perfusable branching microvessel bed for vascularization of engineered tissues. Proc Natl Acad Sci U S A. 2012; 109(50):E3414–23. [PubMed: 23184971]
12. Taboas JM, Maddox RD, Krebsbach PH, Hollister SJ. Indirect solid free form fabrication of local and global porous, biomimetic and composite 3D polymer-ceramic scaffolds. Biomaterials. 2003; 24(1):181–94. [PubMed: 12417192]
13. Kloeters O, Berger I, Ryssel H, Megerle K, Leimer U, Germann G. Revitalization of cortical bone allograft by application of vascularized scaffolds seeded with osteogenic induced adipose tissue derived stem cells in a rabbit model. Arch Orthop Trauma Surg. 2011; 131(10):1459–66. [PubMed: 21594572]
14. Singh S, Wu BM, Dunn JCY. Accelerating vascularization in polycaprolactone scaffolds by endothelial progenitor cells. Tissue Eng Part A. 2011; 17(13 and 14):1819–30. [PubMed: 21395445]
15. Li Q, Wang Z. Influence of mesenchymal stem cells with endothelial progenitor cells in co-culture on osteogenesis and angiogenesis: an in vitro study. Arch Med Res. 2013:1–10.
16. Song JJ, Ott HC. Organ engineering based on decellularized matrix scaffolds. Trends Mol Med. 2011; 17(8):424–32. [PubMed: 21514224]
17. Mertsching H, Schanz J, Steger V, Schandar M, Schenk M, Hansmann J, et al. Generation and transplantation of an autologous vascularized bioartificial human tissue. Transplantation. 2009; 88(2):203–10. [PubMed: 19623015]
18. Charoenpanich A, Wall ME, Tucker CJ, Andrews DMK, Lalush DS, Dirschl DR, et al. Cyclic tensile strain enhances osteogenesis and angiogenesis in mesenchymal stem cells from osteoporotic donors. Tissue Eng Part A. 2014; 20 (00).
19. Oh SH, Ward CL, Atala A, Yoo JJ, Harrison BS. Oxygen generating scaffolds for enhancing engineered tissue survival. Biomaterials. 2009; 30(5):757–62. [PubMed: 19019425]
20. Kaihara S, Borenstein J, Koka R, Lalan S, Ochoa ER, Ravens M, et al. Silicon micromachining to tissue engineer branched vascular channels for liver fabrication. Tissue Eng. 2000; 6(2):105–17. [PubMed: 10941206]
21. Karageorgiou V, Kaplan D. Porosity of 3D biomaterial scaffolds and osteogenesis. Biomaterials. 2005; 26(27):5474–91. [PubMed: 15860204]
22. Harvey EJ, Bobyn JD, Tanzer M, Stackpool GJ, Krygier JJ, Hacking SA. Effect of flexibility of the femoral stem on bone-remodeling and fixation of the stem in a canine total hip arthroplasty model without cement. J Bone Joint Surg Am. 1999; 81(1):93–107. [PubMed: 9973059]
23. Hutmacher DW. Scaffolds in tissue engineering bone and cartilage. Biomaterials. 2000; 21(24): 2529–43. [PubMed: 11071603]
24. Woodfield TBF, Malda J, de Wijn J, Péters F, Riesle J, van Blitterswijk CA. Design of porous scaffolds for cartilage tissue engineering using a three-dimensional fiber-deposition technique. Biomaterials. 2004; 25(18):4149–61. [PubMed: 15046905]
25. Wu S, Liu Y, Bharadwaj S, Atala A, Zhang Y. Human urine-derived stem cells seeded in a modified 3D porous small intestinal submucosa scaffold for urethral tissue engineering. Biomaterials. 2011; 32(5):1317–26. [PubMed: 21055807]
26. Yang J, Chung TW, Nagaoka M, Goto M, Cho C, Akaike T. Hepatocyte-specific porous polymer-scaffolds of alginate / galactosylated chitosan sponge for liver-tissue engineering. Biotechnol Lett. 2001; 23:1385–9.
27. Ma L, Gao C, Mao Z, Zhou J, Shen J, Hu X, et al. Collagen/chitosan porous scaffolds with improved biostability for skin tissue engineering. Biomaterials. 2003; 24(26):4833–41. [PubMed: 14530080]
28. Dagalakis N, Flinkt J, Stasikelis P, Burke JF, Yannass IV. Design of an artificial skin. Part III. Control of pore structure. J Biomed Mater Res. 1980; 14(4):511–28. [PubMed: 7400201]
29. Levenberg S, Rouwkema J, Macdonald M, Garfein ES, Kohane DS, Darland DC, et al. Engineering vascularized skeletal muscle tissue. Nat Biotechnol. 2005; 23(7):879–84. [PubMed: 15965465]

NIH-PA Author Manuscript

NIH-PA Author Manuscript

NIH-PA Author Manuscript

30. Guan J, Fujimoto KL, Sacks MS, Wagner WR. Preparation and characterization of highly porous, biodegradable polyurethane scaffolds for soft tissue applications. Biomaterials. 2005; 26(18): 3961–71. [PubMed: 15626443]

31. Madihally SV, Matthew HW. Porous chitosan scaffolds for tissue engineering. Biomaterials. 1999; 20(12):1133–42. [PubMed: 10382829]

32. Joshi VS, Lei NY, Walthers CM, Wu B, Dunn JCY. Macroporosity enhances vascularization of electrospun scaffolds. J Surg Res. 2013; 183(1):18–26. [PubMed: 23769018]

33. Hollister SJ. Porous scaffold design for tissue engineering. Nat Mater. 2005; 4(7):518–24. [PubMed: 16003400]

34. Bines JE. Intestinal failure: A new era in clinical management. J Gastroenterol Hepatol. 2009; 24(Suppl 3):S86–92. [PubMed: 19799705]

35. Donohoe CL, Reynolds JV. Short bowel syndrome. Surgeon. 2010; 8(5):270–9. [PubMed: 20709285]

36. Wales PW, Christison-Lagay ER. Short bowel syndrome: epidemiology and etiology. Semin Pediatr Surg. 2010; 19(1):3–9. [PubMed: 20123268]

37. Sato T, Vries RG, Snippert HJ, van de Wetering M, Barker N, Stange DE, et al. Single Lgr5 stem cells build crypt-villus structures in vitro without a mesenchymal niche. Nature. 2009; 459(7244): 262–5. [PubMed: 19329995]

38. Jabaji Z, Sears CM, Brinkley GJ, Lei NY, Joshi VS, Wang J, et al. Use of collagen gel as an alternative extracellular matrix for the in vitro and in vivo growth of murine small intestinal epithelium. Tissue Eng Part C Methods. 2013; 19(12):961–69. [PubMed: 23566043]

39. Sala FG, Kunisaki SM, Ochoa ER, Vacanti J, Grikscheit TC. Tissue-engineered small intestine and stomach form from autologous tissue in a preclinical large animal model. J Surg Res. 2009; 156(2):205–12. [PubMed: 19665143]

40. Moon DG, Christ G, Stitzel JD, Atala A, Yoo JJ. Cyclic mechanical preconditioning improves engineered muscle contraction. Tissue Eng Part A. 2008; 14(4):473–82. [PubMed: 18399787]

41. Carrier RL, Rupnick M, Langer R, Schoen FJ, Freed LE, Vunjak-Novakovic G. Perfusion improves tissue architecture of engineered cardiac muscle. Tissue Eng. 2002; 8(2):175–88. [PubMed: 12031108]

42. Lee M, Wu BM, Stelzner M, Reichardt HM, Dunn JCY. Intestinal smooth muscle cell maintenance by basic fibroblast growth factor. Tissue Eng Part A. 2008; 14(8):1395–402. [PubMed: 18680389]

43. Miyasaka EA, Raghavan S, Gilmont RR, Mittal K, Somara S, Bitar KN, et al. In vivo growth of a bioengineered internal anal sphincter: comparison of growth factors for optimization of growth and survival. Pediatr Surg Int. 2011; 27(2):137–43. [PubMed: 21046117]

44. Lee M, Wu BM, Stelzner M, Reichardt HM, Dunn JCY. Intestinal smooth muscle cell maintenance by basic fibroblast growth factor. Tissue Eng Part A. 2008; 14(8):1395–402. [PubMed: 18680389]

45. Geisbauer CL, Chapin JC, Wu BM, Dunn JCY. Transplantation of enteric cells expressing p75 in the rodent stomach. J Surg Res. 2012; 174(2):257–65. [PubMed: 21324400]

46. Cha JM, Park S-N, Noh SH, Suh H. Time-dependent modulation of alignment and differentiation of smooth muscle cells seeded on a porous substrate undergoing cyclic mechanical strain. Artif Organs. 2006; 30(4):250–8. [PubMed: 16643383]

47. Li W-J, Tuli R, Huang X, Laquerriere P, Tuan RS. Multilineage differentiation of human mesenchymal stem cells in a three-dimensional nanofibrous scaffold. Biomaterials. 2005; 26(25): 5158–66. [PubMed: 15792543]

48. Whited BM, Whitney JR, Hofmann MC, Xu Y, Rylander MN. Pre-osteoblast infiltration and differentiation in highly porous apatite-coated PLLA electrospun scaffolds. Biomaterials. 2011; 32(9):2294–304. [PubMed: 21195474]

49. English A, Azeem A, Gaspar DA, Keane K, Kumar P, Keeney M, et al. Preferential cell response to anisotropic electro-spun fibrous scaffolds under tension-free conditions. J Mater Sci Mater Med. 2012; 23(1):137–48. [PubMed: 22105221]

50. Lee CH, Shin HJ, Cho IH, Kang Y-M, Kim IA, Park K-D, et al. Nanofiber alignment and direction of mechanical strain affect the ECM production of human ACL fibroblast. Biomaterials. 2005; 26(11):1261–70. [PubMed: 15475056]

NIH-PA Author Manuscript

NIH-PA Author Manuscript

NIH-PA Author Manuscript

51. Guex AG, Kocher FM, Fortunato G, Körner E, Hegemann D, Carrel TP, et al. Fine-tuning of substrate architecture and surface chemistry promotes muscle tissue development. Acta Biomater. 2012; 8(4):1481–9. [PubMed: 22266032]

52. Schnell E, Klinkhammer K, Balzer S, Brook G, Klee D, Dalton P, et al. Guidance of glial cell migration and axonal growth on electrospun nanofibers of poly-epsilon-caprolactone and a collagen/poly-epsilon-caprolactone blend. Biomaterials. 2007; 28(19):3012–25. [PubMed: 17408736]

53. Li W-J, Laurencin CT, Caterson EJ, Tuan RS, Ko FK. Electrospun nanofibrous structure: a novel scaffold for tissue engineering. J Biomed Mater Res. 2002; 60(4):613–21. [PubMed: 11948520]

54. Phipps MC, Clem WC, Grunda JM, Clines GA, Bellis SL. Increasing the pore sizes of bone-mimetic electrospun scaffolds comprised of polycaprolactone, collagen I and hydroxyapatite to enhance cell infiltration. Biomaterials. 2012; 33(2):524–34. [PubMed: 22014462]

55. Tommasini SM, Wearne SL, Hof PR, Jepsen KJ. Percolation theory relates corticocancellous architecture to mechanical function in vertebrae of inbred mouse strains. Bone. 2008; 42(4):743–50. [PubMed: 18258502]

56. Stauffer, D.; Aharony, A. Introduction to Percolation Theory. 2nd Edition. Taylor & Francis, LTD.; London: 1994.

NIH-PA Author Manuscript
NIH-PA Author Manuscript
NIH-PA Author Manuscript

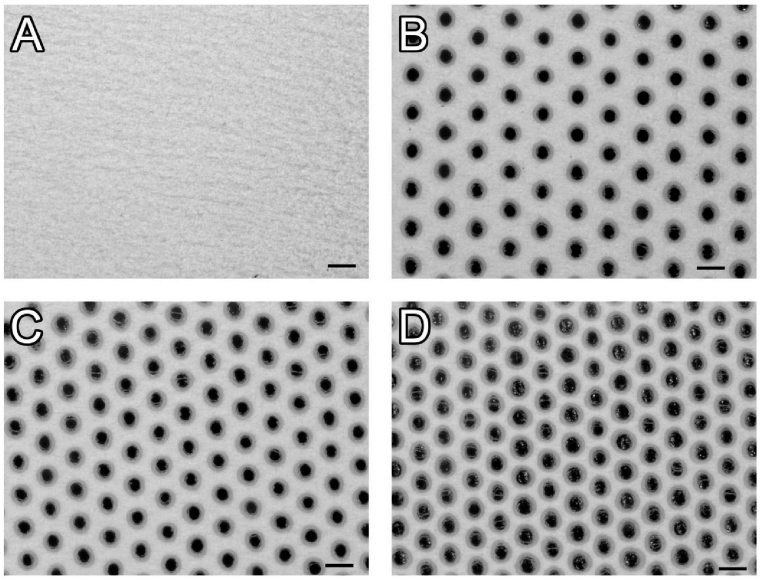

Figure 1.

Macroscopic evaluation of scaffold porosity. Electrospun sheets are white 250-μm holes appear black with a light gray ring of melted polymer around the edge. Mean porosities were measured with ImageJ software and are listed with standard deviations (n=3) in results. Scale bar is 500-μm.

NIH-PA Author Manuscript
NIH-PA Author Manuscript
NIH-PA Author Manuscript

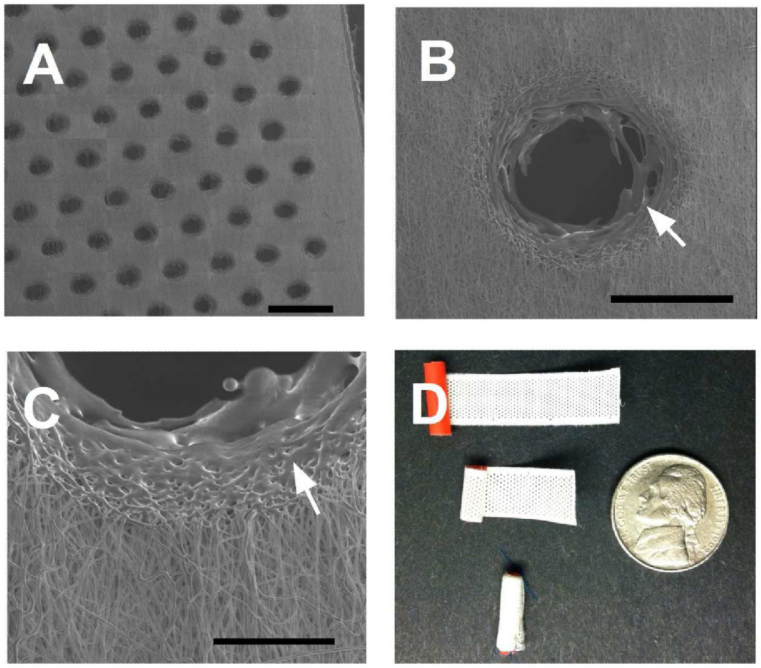

Figure 2.

Scanning electron microscope images of electrospun scaffolds with lasercut macropores. Electrospun sheets, 25% porous, have fiber diameters of about 3-μm and micropore diameters of 250-μm. A dense ring of melted fibers about 75-μm thick forms around the macropores (arrows). Electrospun fibers are aligned vertically. Scale bar is 1000-μm (A), 250-μm (B), and 100-μm (C). The scaffold wrapping process is demonstrated (D) with a nickel for scale.

NIH-PA Author Manuscript

NIH-PA Author Manuscript

NIH-PA Author Manuscript

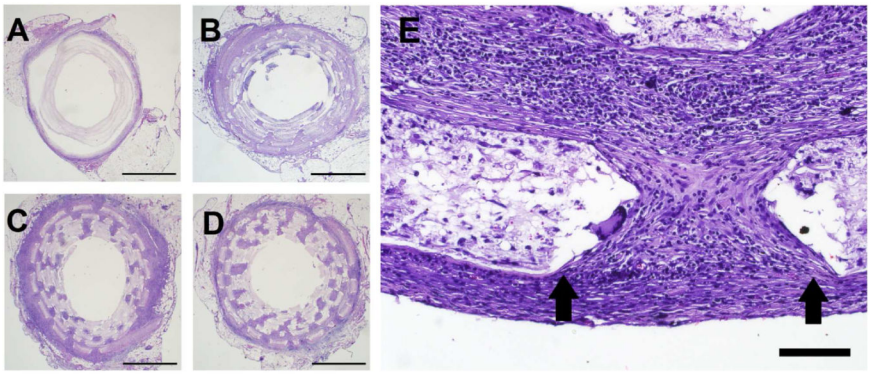

Figure 3.

Hematoxylin and eosin staining of implant sections for 0% porous (A), 15% porous (B), 20% porous (C), and 25% porous (D). Scaffolds were harvested at two weeks and visualized in cross-section with H&E staining. Scaffolds with pores had robust cell infiltration, while the non-porous control shows very little cellular penetration past the outer layer, leading to poor histological processing. Scale bar is 2-mm. A 200x magnification of the 25% porous scaffold (E) shows low cell infiltration within the electrospun fibers due to scaffold density. Cells can be seen aligning along the scaffold fibers. The arrows point to melted polymer ring formed around the laser cut hole. Scale bar is 100-μm.

NIH-PA Author Manuscript
NIH-PA Author Manuscript
NIH-PA Author Manuscript

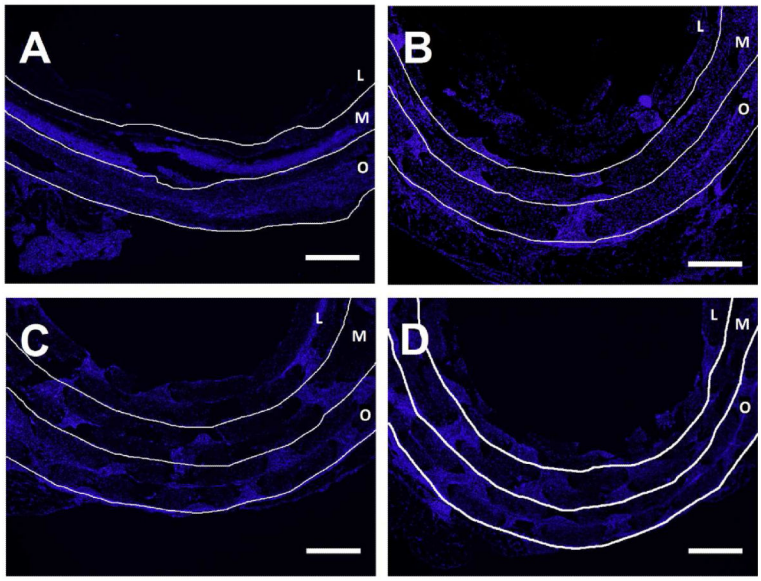

Figure 4.

Cellular penetration measured with DAPI staining. Nuclei were stained with DAPI to visualize cellular penetration through scaffold layers of 0% porous (A), 15% porous (B), 20% porous (C), and 25% porous (D) scaffolds. Representative white lines are drawn to separate the scaffold layers in to outer (layers 5 and 6, O); middle (layers 3 and 4, M); and luminal (layers 1 and 2, L). Scale bar is 500-μm.

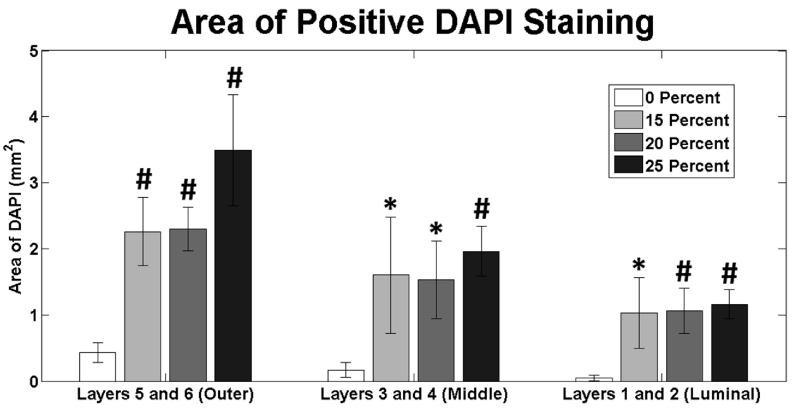

Figure 5.

Quantification of DAPI staining. There was no measurable difference in DAPI staining between layers of the porous implants. All porous implants had a significant improvement in DAPI staining compared to non-porous controls ($p<.05$, *); ($p<.005$, #).

NIH-PA Author Manuscript NIH-PA Author Manuscript NIH-PA Author Manuscript

NIH-PA Author Manuscript
NIH-PA Author Manuscript
NIH-PA Author Manuscript

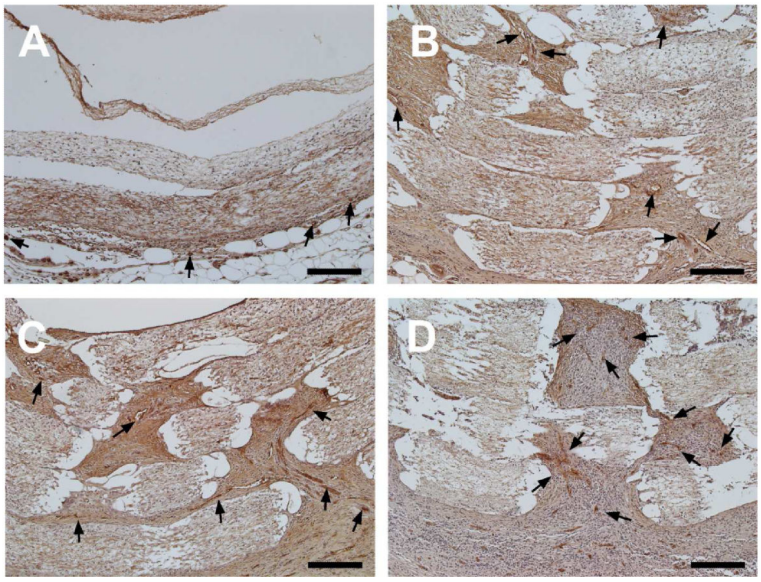

Figure 6.

Immunohistochemical evaluation of implants for von Willebrand Factor positive blood vessels. Angiogenesis was quantified by staining scaffold sections with diaminobenzidine stain and anti-vWF and counter-staining with hematoxylin. A continuous increase in blood vessel numbers corresponded to an increase in macroporosity from 0% porous (A), 15% porous (B), 20% porous (C), and 25% porous (D). Black arrows highlight vWF-stained vessels. Scale bar is 200-μm.

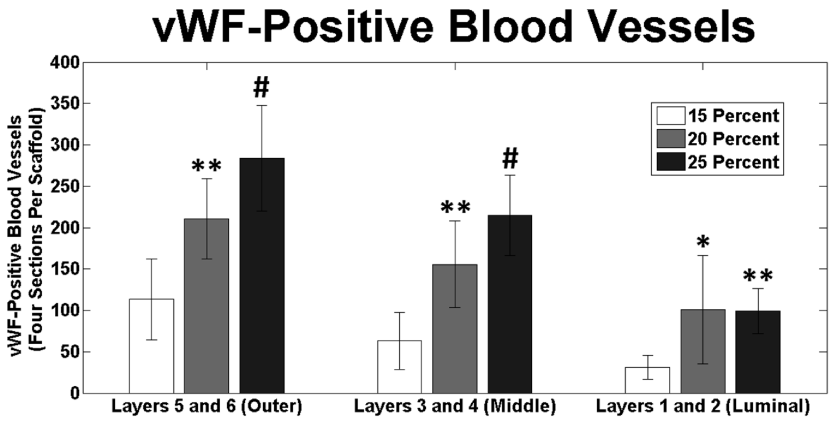

Figure 7.

Quantification of von-Willebrand Factor positive blood vessels. Statistical increases in blood vessel infiltration existed between the 15% scaffolds and all layers of both 20% and 25% macroporous scaffolds ($p<.05$, *; $p<.005$, **). Statistical increases in blood vessel penetration also existed between the 20% and 25% macroporous scaffolds in both the outer and middle layers ($p<.05$, #), but not the luminal layers.

NIH-PA Author Manuscript
NIH-PA Author Manuscript
NIH-PA Author Manuscript

NIH-PA Author Manuscript

NIH-PA Author Manuscript

NIH-PA Author Manuscript

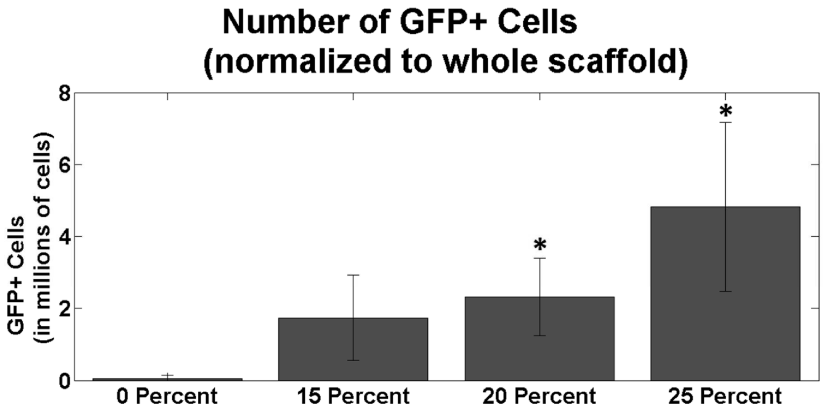

Figure 8.

Green fluorescent protein positive DNA quantified by qPCR. Only the 20% and 25% macroporous scaffolds had a significant increase in GFP+ DNA compared to the non-porous controls.

NIH-PA Author Manuscript
NIH-PA Author Manuscript
NIH-PA Author Manuscript

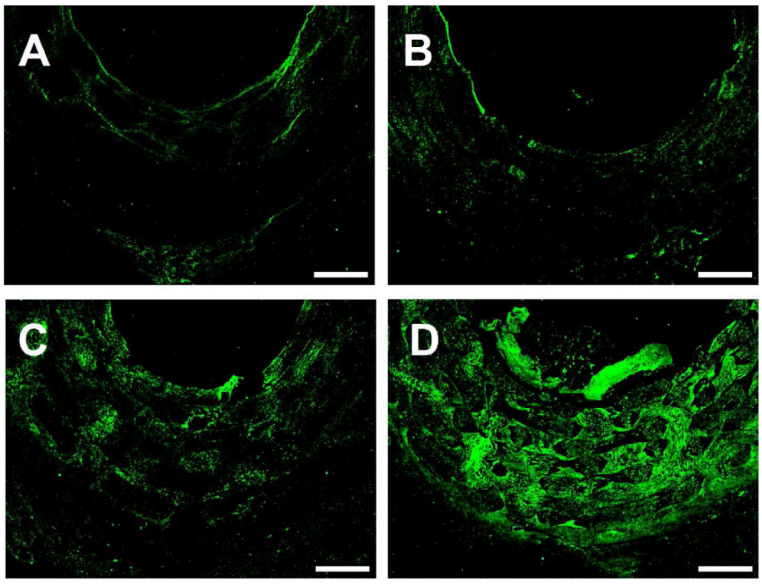

Figure 9.

Immunofluorescent staining for Green Fluorescent Protein. Survival of implanted GFP+ smooth muscle cells was quantified with green fluorescent anti-GFP staining. Few GFP+ cells are noticeable in the 0% porous (A), 15% porous (B), and 20% porous (C) scaffolds, while an increase in fluorescent green GFP+ cells is noticeable in laser cut holes in the 25% porous scaffold (D). Scale bar is 500-μm.

NIH-PA Author Manuscript

NIH-PA Author Manuscript

NIH-PA Author Manuscript

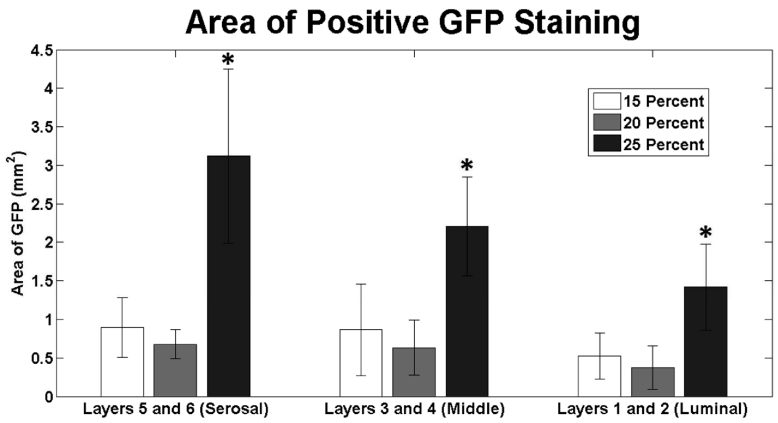

Figure 10.

Quantification of GFP+ staining. Immunofluorescent anti-GFP staining was quantified with ImageJ software. A significant increase in GFP staining was observed in the 25% porous scaffolds compared to both 15% and 20% in all layers ($p<.05$, *). There was no difference between the 15% and 20% porous groups.